Preprints of the 19th World Congress
The International Federation of Automatic Control
Cape Town, South Africa. August 24-29, 2014

Nonlinear Robust Adaptive Control for Spacecraft Proximity Operations ⋆

Liang Sun * **Wei Huo** *

* *The Seventh Research Division*
Science and Technology on Aircraft Control Laboratory
Beihang University, Beijing, 100191, China
(e-mail: sunliang@asee.buaa.edu.cn; weihuo@buaa.edu.cn)

Abstract: The relative motion control for an uncertain chaser spacecraft to approach a tumbling space target is investigated in this paper. The nonlinear coupled dynamics for relative translational and rotational motions of the two spacecrafts are modeled. Based on the model, relative position and attitude controllers are designed by a unified nonlinear robust adaptive control method without using the target inertial parameter information. Asymptotic stability of the six degrees-of-freedom closed-loop system is proved. Theoretical results are demonstrated by a numerical simulation.

Keywords: Spacecraft control, proximity operations, adaptive control, robust control.

1. INTRODUCTION

Many space programs such as rendezvous and docking, capturing, repairing and fueling, tracking various space objects, and removing debris in orbit have attracted a lot of attention in recent years. Autonomous proximity operations in these programs is the most critical technology, it requires precise position and attitude control. Since the relative motion dynamics between two spacecrafts are highly nonlinear and strongly coupled, many classical linear control methods are not applicable.

Various nonlinear controllers have been designed based on the spacecraft relative motion model. A robust controller, including both relative position and relative attitude controls, was designed by Stansbery and Cloutier (2000) for the spacecraft proximity operations with state-dependent Riccati equation technology. Relative position control based on phase plane control technique and relative attitude control based on relative quaternion feedback scheme were developed in Philip and Ananthasayanam (2003). Singla et al. (2006) proposed an output feedback adaptive control to solve the spacecraft autonomous rendezvous and docking problem under measurement noises, but the couplings of relative position and relative attitude motions were not considered. The integrated relative position and attitude control problem for spacecraft proximity operations with parametric uncertainties, bounded disturbances and measurement noises was investigated in Subbarao and Welsh (2008), and ultimate boundedness of the closed-loop system errors was achieved. In Di Cairano et al. (2010), the relative position control problem for spacecraft proximity operations was converted to a model predictive control optimization problem with considering thrust magnitude and spacecraft approach velocity constraints. Liang and Ma (2011) proposed a Lyapunov-based adaptive control method for tracking the angular velocity of a tumbling satellite before docking and stabilizing rotation of the two-satellite compound system after docking. By the use of the method, only the rotational motion can be stabilized, but the coupled relative translational motion was not considered as in Meng et al. (2010). Xin and Pan (2010) addressed a closed-form nonlinear optimal control solution for spacecraft proximity operations with θ-D technique. Although the relative position and attitude dynamics coupled with the flexible appendage were used to design a unified optimal controller, the parametric uncertainties and external disturbances were not considered. Then they researched again the problem in Xin and Pan (2012) and redesigned the optimal controller with considering the modeling uncertainties. Zhang et al. (2012) designed the integrated relative position and attitude controller for a chaser spacecraft with control saturation, but the target attitude information is required in real time.

In light of above achievements, we consider the problem of positioning a chaser spacecraft to a desired proximity position along the docking port direction of a space target, and synchronizing the chaser attitude with the tumbling target attitude. The main contribution of the paper is as follows. First, the relative translational and rotational motions are all modeled in the chaser spacecraft body-fixed frame. Although the two relative motions are coupled in the model, relative position controller and relative attitude controller are independently designed by a unified nonlinear robust adaptive control method without using the target inertial parameter information. Second, in spite of the decoupled controller design, asymptotic stability of the closed-loop system for spacecraft proximity operations is proved based on the coupled six degrees-of-freedom dynamics model.

This paper is arranged as follows. In section 2, the mechanical model of the spacecraft proximity operations is derived, and the objective of controller design is stated. In section 3, detailed designing procedure of a robust adaptive nonlinear state feedback controller is proposed, and stability analysis of the closed-loop system is presented in section 4. Simulation results are then shown in section 5. Finally, conclusion is given in section 6.

⋆ This work was supported by the National Natural Science Foundation of China under grant 61134005 and the National Basic Research Program of China (973 Program) under grant 2012CB821204.

2. MODELING AND PROBLEM DESCRIPTION

Notations. The skew symmetric matrix $S(\boldsymbol{a}) \in \mathbb{R}^{3\times3}$ derived from a vector $\boldsymbol{a} = [a_1, a_2, a_3]^{\mathrm{T}} \in \mathbb{R}^3$ is defined as

$$S(\boldsymbol{a}) = \begin{bmatrix} 0 & -a_3 & a_2 \\ a_3 & 0 & -a_1 \\ -a_2 & a_1 & 0 \end{bmatrix}$$

It satisfies $\|S(\boldsymbol{a})\| = \|\boldsymbol{a}\|$, $\boldsymbol{a}^{\mathrm{T}}S(\boldsymbol{a}) = 0$, and $S(\boldsymbol{a})\boldsymbol{b} = -S(\boldsymbol{b})\boldsymbol{a}$, $\boldsymbol{b}^{\mathrm{T}}S(\boldsymbol{a})\boldsymbol{b} = 0$ for any $\boldsymbol{b} \in \mathbb{R}^3$. Moreover, $\|\boldsymbol{a}\| \le \|\boldsymbol{a}\|_1$, where $\|\boldsymbol{a}\|$ and $\|\boldsymbol{a}\|_1$ denote vector 2-norm and 1-norm, respectively. $A > 0$ represents that A is a positive definite matrix, and $\|A\|$ is its induced matrix 2-norm. $\mathrm{sgn}(\boldsymbol{a}) \triangleq [\mathrm{sgn}(a_1), \mathrm{sgn}(a_2), \mathrm{sgn}(a_3)]^{\mathrm{T}}$, where

$$\mathrm{sgn}(a_i) = \begin{cases} -1, & a_i < 0 \\ 0, & a_i = 0 \\ 1, & a_i > 0 \end{cases}$$

2.1 Chaser and Target Dynamics

The control problem that a chaser spacecraft with modeling uncertainties tracks a tumbling space target is considered in this paper. Relevant frames and vectors are shown in Figure 1, where $\mathscr{F}_i \triangleq \{\mathbf{O}x_iy_iz_i\}$ is an Earth-centered inertial frame, $\mathscr{F}_c \triangleq \{\mathbf{C}xyz\}$ and $\mathscr{F}_t \triangleq \{\mathbf{T}x_ty_tz_t\}$ are the chaser and target body-fixed frames, and their origins **C** and **T** are mass centers of the chaser and target, respectively. Point **P** is the chaser desired proximity position along direction of the target docking port. Solid arrows $\{\boldsymbol{r}, \boldsymbol{r}_e\}$ and dashed arrows $\{\boldsymbol{r}_t, \boldsymbol{r}_{p_t}, \boldsymbol{p}_t\}$ are the vectors represented in frame $\mathscr{F}_c$ and frame $\mathscr{F}_t$, respectively. The task of this work is to control the chaser spacecraft such that point **C** tracks point **P** and frame $\mathscr{F}_c$ tracks frame $\mathscr{F}_t$.

The position of mass center **C** and the attitude of frame $\mathscr{F}_c$ with respect to frame $\mathscr{F}_i$ can be described by following chaser kinematics and dynamics equations expressed in frame $\mathscr{F}_c$, if the modified Rodrigues parameters(MRP) are used for attitude parametrization (Xin and Pan (2011)):

$$\dot{\boldsymbol{r}} = \boldsymbol{v} - S(\boldsymbol{\omega})\boldsymbol{r} \tag{1}$$

$$\dot{\boldsymbol{\sigma}} = \frac{1}{4}[(1-\boldsymbol{\sigma}^{\mathrm{T}}\boldsymbol{\sigma})I_3 + 2S(\boldsymbol{\sigma}) + 2\boldsymbol{\sigma}\boldsymbol{\sigma}^{\mathrm{T}}]\boldsymbol{\omega} \tag{2}$$

$$m\dot{\boldsymbol{v}} + mS(\boldsymbol{\omega})\boldsymbol{v} = \boldsymbol{f} + \boldsymbol{d}_f \tag{3}$$

$$J\dot{\boldsymbol{\omega}} + S(\boldsymbol{\omega})J\boldsymbol{\omega} = \boldsymbol{\tau} + \boldsymbol{d}_\tau \tag{4}$$

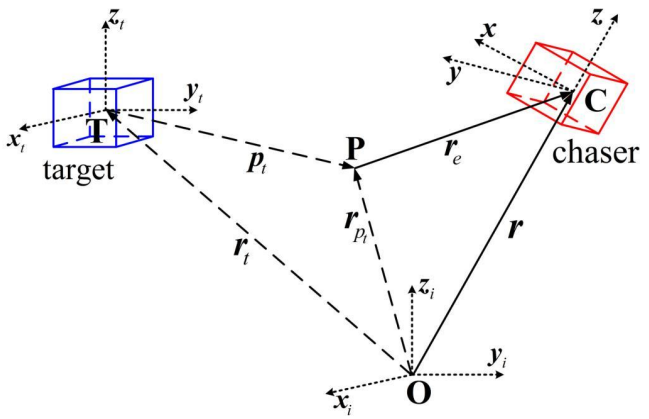

Fig. 1. Relevant frames and vectors

where $\boldsymbol{r} \in \mathbb{R}^3$ is the position and $\boldsymbol{\sigma}$ is the MRP attitude with the constraint $\|\boldsymbol{\sigma}\| \le 1$; $\boldsymbol{v}, \boldsymbol{\omega} \in \mathbb{R}^3$ are linear and angular velocities; $\boldsymbol{f}, \boldsymbol{\tau}, \boldsymbol{d}_f, \boldsymbol{d}_\tau \in \mathbb{R}^3$ are the control force, control torque, disturbance force and disturbance torque, respectively; $m \in \mathbb{R}$ and $J \in \mathbb{R}^{3\times3}$ are the chaser mass and inertia matrix. I_3 is a 3×3 unit matrix.

With the same description manner for the chaser motion, the kinematics and dynamics for target translational and rotational motions are described in frame $\mathscr{F}_t$ as

$$\dot{\boldsymbol{r}}_t = \boldsymbol{v}_t - S(\boldsymbol{\omega}_t)\boldsymbol{r}_t \tag{5}$$

$$\dot{\boldsymbol{\sigma}}_t = \frac{1}{4}[(1-\boldsymbol{\sigma}_t^{\mathrm{T}}\boldsymbol{\sigma}_t)I_3 + 2S(\boldsymbol{\sigma}_t) + 2\boldsymbol{\sigma}_t\boldsymbol{\sigma}_t^{\mathrm{T}}]\boldsymbol{\omega}_t \tag{6}$$

$$m_t\dot{\boldsymbol{v}}_t + m_tS(\boldsymbol{\omega}_t)\boldsymbol{v}_t = \boldsymbol{0} \tag{7}$$

$$J_t\dot{\boldsymbol{\omega}}_t + S(\boldsymbol{\omega}_t)J_t\boldsymbol{\omega}_t = \boldsymbol{0} \tag{8}$$

where $\boldsymbol{r}_t, \boldsymbol{\sigma}_t \in \mathbb{R}^3$ are target position and attitude; $\boldsymbol{v}_t, \boldsymbol{\omega}_t \in \mathbb{R}^3$ are target linear and angular velocities; $m_t \in \mathbb{R}$ and $J_t \in \mathbb{R}^{3\times3}$ are target mass and positive definite symmetric inertia matrix, respectively.

Claim 1. For the target dynamics (7) and (8), denote target kinetic energy $E(t) = \frac{1}{2}(m_t\boldsymbol{v}_t^{\mathrm{T}}\boldsymbol{v}_t + \boldsymbol{\omega}_t^{\mathrm{T}}J_t\boldsymbol{\omega}_t) \ge 0$, since its time derivative $\dot{E}(t) = -m_t\boldsymbol{v}_t^{\mathrm{T}}S(\boldsymbol{\omega}_t)\boldsymbol{v}_t - \boldsymbol{\omega}_t^{\mathrm{T}}S(\boldsymbol{\omega}_t)J_t\boldsymbol{\omega}_t \equiv 0$, we know that $E(t) \equiv E(0) \triangleq \frac{1}{2}(m_t\boldsymbol{v}_t^{\mathrm{T}}(0)\boldsymbol{v}_t(0) + \boldsymbol{\omega}_t^{\mathrm{T}}(0)J_t\boldsymbol{\omega}_t(0)) < \infty$. Therefore, the target linear velocity $\boldsymbol{v}_t$ and angular velocity $\boldsymbol{\omega}_t$ are always bounded.

2.2 Relative Motion Dynamics

The rotation matrix from $\mathscr{F}_t$ to $\mathscr{F}_c$ is (Shuster (1993))

$$R = I_3 - \frac{4(1-\boldsymbol{\sigma}_e^{\mathrm{T}}\boldsymbol{\sigma}_e)}{(1+\boldsymbol{\sigma}_e^{\mathrm{T}}\boldsymbol{\sigma}_e)^2}S(\boldsymbol{\sigma}_e) + \frac{8}{(1+\boldsymbol{\sigma}_e^{\mathrm{T}}\boldsymbol{\sigma}_e)^2}S(\boldsymbol{\sigma}_e)^{\mathrm{T}}S(\boldsymbol{\sigma}_e) \tag{9}$$

where $\boldsymbol{\sigma}_e$ is the MRP of relative attitude defined by

$$\boldsymbol{\sigma}_e = \frac{\boldsymbol{\sigma}_t(\boldsymbol{\sigma}^{\mathrm{T}}\boldsymbol{\sigma} - 1) + \boldsymbol{\sigma}(1 - \boldsymbol{\sigma}_t^{\mathrm{T}}\boldsymbol{\sigma}_t) - 2S(\boldsymbol{\sigma}_t)\boldsymbol{\sigma}}{1 + \boldsymbol{\sigma}_t^{\mathrm{T}}\boldsymbol{\sigma}_t\boldsymbol{\sigma}^{\mathrm{T}}\boldsymbol{\sigma} + 2\boldsymbol{\sigma}_t^{\mathrm{T}}\boldsymbol{\sigma}} \tag{10}$$

According to Figure 1, the position and velocity of point **P** can be described in frame $\mathscr{F}_t$ as

$$\boldsymbol{r}_{p_t} = \boldsymbol{r}_t + \boldsymbol{p}_t, \qquad \boldsymbol{v}_{p_t} = \boldsymbol{v}_t + S(\boldsymbol{\omega}_t)\boldsymbol{p}_t \tag{11}$$

where $\boldsymbol{p}_t \in \mathbb{R}^3$ is a constant vector in frame $\mathscr{F}_t$. The relative position, relative linear and angular velocities are all represented in frame $\mathscr{F}_c$ as

$$\boldsymbol{r}_e = \boldsymbol{r} - R\boldsymbol{r}_{p_t}, \quad \boldsymbol{v}_e = \boldsymbol{v} - R\boldsymbol{v}_{p_t}, \quad \boldsymbol{\omega}_e = \boldsymbol{\omega} - R\boldsymbol{\omega}_t \tag{12}$$

Substituting (12) into (1)–(4) and using $\dot{R} = -S(\boldsymbol{\omega}_e)R$, $\dot{\boldsymbol{r}}_{p_t} = \boldsymbol{v}_{p_t} - S(\boldsymbol{\omega}_t)\boldsymbol{r}_{p_t}$ and $R^{-1} = R^{\mathrm{T}}$ yield the relative motion models represented in frame $\mathscr{F}_c$ as (Yuichi et al. (2011))

$$\dot{\boldsymbol{r}}_e = \boldsymbol{v}_e - S(\boldsymbol{\omega})\boldsymbol{r}_e \tag{13}$$

$$\dot{\boldsymbol{\sigma}}_e = G(\boldsymbol{\sigma}_e)\boldsymbol{\omega}_e \tag{14}$$

$$m\dot{\boldsymbol{v}}_e = -m[S(\boldsymbol{\omega} - \boldsymbol{\omega}_e)\boldsymbol{v} + S(\boldsymbol{\omega}_e)\boldsymbol{v}_e + R\dot{\boldsymbol{v}}_{p_t}] + \boldsymbol{f} + \boldsymbol{d}_f \tag{15}$$

$$J\dot{\boldsymbol{\omega}}_e = -S(\boldsymbol{\omega})J\boldsymbol{\omega} - J[R\dot{\boldsymbol{\omega}}_t - S(\boldsymbol{\omega}_e)(\boldsymbol{\omega} - \boldsymbol{\omega}_e)] + \boldsymbol{\tau} + \boldsymbol{d}_\tau \tag{16}$$

where $G(\boldsymbol{\sigma}_e) = \frac{1}{4}[(1-\boldsymbol{\sigma}_e^{\mathrm{T}}\boldsymbol{\sigma}_e)I_3 + 2S(\boldsymbol{\sigma}_e) + 2\boldsymbol{\sigma}_e\boldsymbol{\sigma}_e^{\mathrm{T}}]$ is invertible, $R\dot{\boldsymbol{v}}_{p_t}$ can be calculated from (11), (7), (12) and $RS(\boldsymbol{a}) = S(R\boldsymbol{a})R$ for any $\boldsymbol{a} \in \mathbb{R}^3$ as

$$\begin{aligned} R\dot{\boldsymbol{v}}_{p_t} =& R[\dot{\boldsymbol{v}}_t + S(\dot{\boldsymbol{\omega}}_t)\boldsymbol{p}_t] = -RS(\boldsymbol{\omega}_t)\boldsymbol{v}_t - RS(\boldsymbol{p}_t)\dot{\boldsymbol{\omega}}_t \\ =& -S(R\boldsymbol{\omega}_t)[R\boldsymbol{v}_{p_t} - RS(\boldsymbol{\omega}_t)\boldsymbol{p}_t] - RS(\boldsymbol{p}_t)\dot{\boldsymbol{\omega}}_t \\ =& -S(\boldsymbol{\omega} - \boldsymbol{\omega}_e)[\boldsymbol{v} - \boldsymbol{v}_e - S(\boldsymbol{\omega} - \boldsymbol{\omega}_e)R\boldsymbol{p}_t] \\ & - RS(\boldsymbol{p}_t)\dot{\boldsymbol{\omega}}_t \end{aligned} \tag{17}$$

and $\dot{\boldsymbol{\omega}}_t$ is calculated from (8) and (12) as

$$\begin{aligned}\dot{\boldsymbol{\omega}}_t &= -J_t^{-1}S(\boldsymbol{\omega}_t)J_t\boldsymbol{\omega}_t \\ &= -J_t^{-1}S(R^{\mathrm{T}}(\boldsymbol{\omega}-\boldsymbol{\omega}_e))J_tR^{\mathrm{T}}(\boldsymbol{\omega}-\boldsymbol{\omega}_e)\end{aligned} \tag{18}$$

Thus the equations (15) and (16) can be rewritten as

$$m\dot{\boldsymbol{v}}_e = -m\boldsymbol{g} - m\boldsymbol{n}_1 + \boldsymbol{f} + \boldsymbol{d}_f \tag{19}$$

$$J\dot{\boldsymbol{\omega}}_e = -S(\boldsymbol{\omega})J\boldsymbol{\omega} + JS(\boldsymbol{\omega}_e)(\boldsymbol{\omega}-\boldsymbol{\omega}_e) + J\boldsymbol{n}_2 + \boldsymbol{\tau} + \boldsymbol{d}_\tau \tag{20}$$

where

$$\begin{aligned}\boldsymbol{g} =& S(\boldsymbol{\omega})\boldsymbol{v}_e + S^2(\boldsymbol{\omega}-\boldsymbol{\omega}_e)R\boldsymbol{p}_t \\ \boldsymbol{n}_1 =& RS(\boldsymbol{p}_t)J_t^{-1}S(R^{\mathrm{T}}(\boldsymbol{\omega}-\boldsymbol{\omega}_e))J_tR^{\mathrm{T}}(\boldsymbol{\omega}-\boldsymbol{\omega}_e) \\ \boldsymbol{n}_2 =& RJ_t^{-1}S(R^{\mathrm{T}}(\boldsymbol{\omega}-\boldsymbol{\omega}_e))J_tR^{\mathrm{T}}(\boldsymbol{\omega}-\boldsymbol{\omega}_e)\end{aligned}$$

Claim 2. The terms $S(\boldsymbol{\omega})\boldsymbol{r}_e$ in (13) and $\boldsymbol{n}_1$ in (19) reflect that the relative translation between the two spacecrafts is affected greatly by the relative rotation between them. This indicates natural couplings of the spacecraft proximity operations system.

Generally, in above system dynamic models (19) and (20), the chaser mass m, inertia matrix J, external disturbance force $\boldsymbol{d}_f$, disturbance torque $\boldsymbol{d}_\tau$ and the target inertia matrix J_t are unknown. In this paper, following assumptions are adopted in the subsequent development.

Hypothesis 1. $m = m_0 + m_\Delta$ is a positive scalar and $J = J_0 + J_\Delta$ is a symmetric positive definite matrix, where nominal value m_0 is a known positive constant and $J_0 = \mathrm{diag}\{J_{11}^0, J_{22}^0, J_{33}^0\}$ is a known positive diagonal matrix; m_Δ is an unknown and bounded constant, $J_\Delta = [\Delta_{ij}](i,j=1,2,3)$ is an unknown and bounded symmetric matrix. J_t is an unknown and bounded symmetric positive definite matrix.

Hypothesis 2. The disturbances $\boldsymbol{d}_f$ and $\boldsymbol{d}_\tau$ are completely unknown, but they satisfy $\|\boldsymbol{d}_f\| \le \rho_f$ and $\|\boldsymbol{d}_\tau\| \le \rho_\tau$, where ρ_f and ρ_τ are unknown constants.

Hypothesis 3. The chaser desired position $\boldsymbol{p}_t$ represented in frame $\mathscr{F}_t$ is prior known. Moreover, the chaser can directly measure its motion variables $\{\boldsymbol{r}, \boldsymbol{v}, \boldsymbol{\sigma}, \boldsymbol{\omega}\}$ and relative motion variables $\{\boldsymbol{r}_e, \boldsymbol{v}_e, \boldsymbol{\sigma}_e, \boldsymbol{\omega}_e\}$ with the measurement devices mounted on the chaser body (Lither and Dubowsky (2004)). However, the target motion variables $\{\boldsymbol{r}_t, \boldsymbol{v}_e, \boldsymbol{\sigma}_t, \boldsymbol{\omega}_t\}$ are assumed to be unavailable directly for the chaser.

2.3 Control Objective

The objective of this paper is to design a controller based on above relative motion models to drive the chaser to a desired position on direction of the target docking port and reorient the chaser attitude to coincide with the target attitude. Considering (12), the objective is equivalent to design robust nonlinear control inputs $\boldsymbol{f}$ and $\boldsymbol{\tau}$, such that the controlled spacecraft proximity operations system with above-mentioned modeling uncertainties is capable to guarantee $\lim_{t\to\infty}\boldsymbol{r}_e = \lim_{t\to\infty}\boldsymbol{v}_e = \lim_{t\to\infty}\boldsymbol{\sigma}_e = \lim_{t\to\infty}\boldsymbol{\omega}_e = \boldsymbol{0}$.

3. CONTROLLER DESIGN

In this section, a robust adaptive nonlinear control approach is developed for the spacecraft proximity operations. The adaptive control laws are used to compensate the chaser parametric uncertainties and the unknown coupled dynamics of translational and rotational motions, and to suppress the external environment disturbances.

3.1 Relative Position Controller Design

Define a manifold

$$\boldsymbol{s}_1 = \boldsymbol{v}_e + \Lambda_1\boldsymbol{r}_e \tag{21}$$

where $\Lambda_1 = \Lambda_1^{\mathrm{T}} > 0$ is the feedback gain matrix. Differentiating (21) gives

$$\begin{aligned}m\dot{\boldsymbol{s}}_1 &= m\dot{\boldsymbol{v}}_e + m\Lambda_1\dot{\boldsymbol{r}}_e \\ &= -m\boldsymbol{g} - m\boldsymbol{n}_1 + \boldsymbol{f} + \boldsymbol{d}_f + m\Lambda_1\boldsymbol{v}_e - m\Lambda_1S(\boldsymbol{\omega})\boldsymbol{r}_e \\ &= -m\boldsymbol{y} - m\boldsymbol{n}_1 + \boldsymbol{f} + \boldsymbol{d}_f\end{aligned} \tag{22}$$

where $\boldsymbol{y} = \boldsymbol{g} + \Lambda_1\boldsymbol{v}_e + \Lambda_1S(\boldsymbol{\omega})\boldsymbol{r}_e$.

Based on Hypothesis 1 and 2, denoting unknown constant scalar $\rho_m = |m|\|J_t^{-1}\|\|J_t\|$, estimation errors $\tilde{m}_\Delta = \hat{m}_\Delta - m_\Delta$, $\tilde{\rho}_m = \hat{\rho}_m - \rho_m$, $\tilde{\rho}_f = \hat{\rho}_f - \rho_f$, and selecting a function

$$V_1 = \frac{1}{2}k_0\boldsymbol{r}_e^{\mathrm{T}}\boldsymbol{r}_e + \frac{1}{2}m\boldsymbol{s}_1^{\mathrm{T}}\boldsymbol{s}_1 + \frac{1}{2\gamma_1}\tilde{m}_\Delta^2 + \frac{1}{2\gamma_2}\tilde{\rho}_f^2 + \frac{1}{2\gamma_3}\tilde{\rho}_m^2 \tag{23}$$

where $k_0 > 0$ is a constant gain and $\gamma_i > 0 (i = 1,2,3)$; then from (13), (21), (22) and considering $k_0\boldsymbol{r}_e^{\mathrm{T}}S(\boldsymbol{\omega})\boldsymbol{r}_e = 0$, we have

$$\begin{aligned}\dot{V}_1 =& k_0\boldsymbol{r}_e^{\mathrm{T}}\dot{\boldsymbol{r}}_e + \boldsymbol{s}_1^{\mathrm{T}}m\dot{\boldsymbol{s}}_1 + \frac{1}{\gamma_1}\tilde{m}_\Delta\dot{\hat{m}}_\Delta + \frac{1}{\gamma_2}\tilde{\rho}_f\dot{\hat{\rho}}_f + \frac{1}{\gamma_3}\tilde{\rho}_m\dot{\hat{\rho}}_m \\ =& -k_0\boldsymbol{r}_e^{\mathrm{T}}\Lambda_1\boldsymbol{r}_e + \boldsymbol{s}_1^{\mathrm{T}}(k_0\boldsymbol{r}_e - m\boldsymbol{y} - m\boldsymbol{n}_1 + \boldsymbol{f} + \boldsymbol{d}_f) \\ &+ \frac{1}{\gamma_1}\tilde{m}_\Delta\dot{\hat{m}}_\Delta + \frac{1}{\gamma_2}\tilde{\rho}_f\dot{\hat{\rho}}_f + \frac{1}{\gamma_3}\tilde{\rho}_m\dot{\hat{\rho}}_m\end{aligned} \tag{24}$$

Design the relative position control input

$$\begin{aligned}\boldsymbol{f} =& -k_0\boldsymbol{r}_e - K_1\boldsymbol{s}_1 + (m_0 + \hat{m}_\Delta)\boldsymbol{y} - \hat{\rho}_f\mathrm{sgn}(\boldsymbol{s}_1) \\ &- \hat{\rho}_m\|\boldsymbol{p}_t\|\|\boldsymbol{\omega}-\boldsymbol{\omega}_e\|^2\mathrm{sgn}(\boldsymbol{s}_1)\end{aligned} \tag{25}$$

where constant gain matrix $K_1 = K_1^{\mathrm{T}} > 0$. Substituting (25) into (24) gives the derivative of V_1 as

$$\begin{aligned}\dot{V}_1 =& -k_0\boldsymbol{r}_e^{\mathrm{T}}\Lambda_1\boldsymbol{r}_e - \boldsymbol{s}_1^{\mathrm{T}}K_1\boldsymbol{s}_1 + \boldsymbol{s}_1^{\mathrm{T}}\tilde{m}_\Delta\boldsymbol{y} - \boldsymbol{s}_1^{\mathrm{T}}m\boldsymbol{n}_1 + \boldsymbol{s}_1^{\mathrm{T}}\boldsymbol{d}_f \\ &- \boldsymbol{s}_1^{\mathrm{T}}\hat{\rho}_f\mathrm{sgn}(\boldsymbol{s}_1) - \boldsymbol{s}_1^{\mathrm{T}}\hat{\rho}_m\|\boldsymbol{p}_t\|\|\boldsymbol{\omega}-\boldsymbol{\omega}_e\|^2\mathrm{sgn}(\boldsymbol{s}_1) \\ &+ \frac{1}{\gamma_1}\tilde{m}_\Delta\dot{\hat{m}}_\Delta + \frac{1}{\gamma_2}\tilde{\rho}_f\dot{\hat{\rho}}_f + \frac{1}{\gamma_3}\tilde{\rho}_m\dot{\hat{\rho}}_m\end{aligned} \tag{26}$$

If design parameters adaptive update laws as follows:

$$\begin{cases}\dot{\hat{m}}_\Delta = -\gamma_1\boldsymbol{y}^{\mathrm{T}}\boldsymbol{s}_1 \\ \dot{\hat{\rho}}_f = \gamma_2\|\boldsymbol{s}_1\|_1 \\ \dot{\hat{\rho}}_m = \gamma_3\|\boldsymbol{p}_t\|\|\boldsymbol{\omega}-\boldsymbol{\omega}_e\|^2\|\boldsymbol{s}_1\|_1\end{cases} \tag{27}$$

substituting (27) into (26) and using $\|S(\boldsymbol{a})\| = \|\boldsymbol{a}\|$, $\|R\| = \|R^{\mathrm{T}}\| = 1$, $\|\boldsymbol{s}_1\| \le \|\boldsymbol{s}_1\|_1$ result in

$$\begin{aligned}\dot{V}_1 \le& -k_0\boldsymbol{r}_e^{\mathrm{T}}\Lambda_1\boldsymbol{r}_e - \boldsymbol{s}_1^{\mathrm{T}}K_1\boldsymbol{s}_1 + \boldsymbol{s}_1^{\mathrm{T}}\tilde{m}_\Delta\boldsymbol{y} \\ &+ \rho_m\|\boldsymbol{s}_1\|\|R\|\|\boldsymbol{p}_t\|\|R^{\mathrm{T}}\|^2\|\boldsymbol{\omega}-\boldsymbol{\omega}_e\|^2 \\ &+ \rho_f\|\boldsymbol{s}_1\| - \hat{\rho}_f\|\boldsymbol{s}_1\|_1 - \hat{\rho}_m\|\boldsymbol{p}_t\|\|\boldsymbol{\omega}-\boldsymbol{\omega}_e\|^2\|\boldsymbol{s}_1\|_1 \\ &- \tilde{m}_\Delta\boldsymbol{y}^{\mathrm{T}}\boldsymbol{s}_1 + \tilde{\rho}_f\|\boldsymbol{s}_1\|_1 + \tilde{\rho}_m\|\boldsymbol{p}_t\|\|\boldsymbol{\omega}-\boldsymbol{\omega}_e\|^2\|\boldsymbol{s}_1\|_1 \\ \le& -\boldsymbol{s}_1^{\mathrm{T}}K_1\boldsymbol{s}_1 + \rho_m\|\boldsymbol{p}_t\|\|\boldsymbol{\omega}-\boldsymbol{\omega}_e\|^2\|\boldsymbol{s}_1\|_1 + \rho_f\|\boldsymbol{s}_1\|_1 \\ &- \hat{\rho}_f\|\boldsymbol{s}_1\|_1 - \hat{\rho}_m\|\boldsymbol{p}_t\|\|\boldsymbol{\omega}-\boldsymbol{\omega}_e\|^2\|\boldsymbol{s}_1\|_1 \\ &+ \tilde{\rho}_f\|\boldsymbol{s}_1\|_1 + \tilde{\rho}_m\|\boldsymbol{p}_t\|\|\boldsymbol{\omega}-\boldsymbol{\omega}_e\|^2\|\boldsymbol{s}_1\|_1 \\ =& -\boldsymbol{s}_1^{\mathrm{T}}K_1\boldsymbol{s}_1 \le 0\end{aligned}$$

and the closed-loop position dynamics becomes

$$\begin{aligned}m\dot{\boldsymbol{s}}_1 =& -k_0\boldsymbol{r}_e - K_1\boldsymbol{s}_1 + \tilde{m}_\Delta\boldsymbol{y} - m\boldsymbol{n}_1 + \boldsymbol{d}_f \\ &- \hat{\rho}_f\mathrm{sgn}(\boldsymbol{s}_1) - \hat{\rho}_m\|\boldsymbol{p}_t\|\|\boldsymbol{\omega}-\boldsymbol{\omega}_e\|^2\mathrm{sgn}(\boldsymbol{s}_1)\end{aligned} \tag{28}$$

3.2 Relative Attitude Controller Design

Define a manifold

$$\boldsymbol{s}_2 = \boldsymbol{\omega}_e + \Lambda_2\boldsymbol{\sigma}_e \tag{29}$$

where feedback gain matrix $\Lambda_2 = \Lambda_2^{\mathrm{T}} > 0$, from (29), (16), (14) and (8), we get

$$\begin{aligned} J\dot{\boldsymbol{s}}_2 =& J\dot{\boldsymbol{\omega}}_e + J\Lambda_2\dot{\boldsymbol{\sigma}}_e \\ =& -S(\boldsymbol{\omega})J\boldsymbol{\omega} + JS(\boldsymbol{\omega}_e)(\boldsymbol{\omega}-\boldsymbol{\omega}_e) + J\Lambda_2 G(\boldsymbol{\sigma}_e)\boldsymbol{\omega}_e \\ &+ \boldsymbol{\tau} + \boldsymbol{d}_\tau + JRJ_t^{-1}S(R^{\mathrm{T}}(\boldsymbol{\omega}-\boldsymbol{\omega}_e))J_tR^{\mathrm{T}}(\boldsymbol{\omega}-\boldsymbol{\omega}_e) \end{aligned} \tag{30}$$

From Hypothesis 1 and 2, introduce a linear operator $L(\boldsymbol{a})$ for any vector $\boldsymbol{a} = [a_1, a_2, a_3]^{\mathrm{T}}$ as

$$L(\boldsymbol{a}) \triangleq \begin{bmatrix} a_1 & 0 & 0 & 0 & a_3 & a_2 \\ 0 & a_2 & 0 & a_3 & 0 & a_1 \\ 0 & 0 & a_3 & a_2 & a_1 & 0 \end{bmatrix}$$

we have $J\boldsymbol{a} = L(\boldsymbol{a})\boldsymbol{\theta} = L(\boldsymbol{a})(\boldsymbol{\theta}_0 + \boldsymbol{\theta}_\Delta)$, where $\boldsymbol{\theta} \triangleq [J_{11}, J_{22}, J_{33}, J_{23}, J_{13}, J_{12}]^{\mathrm{T}}$, $\boldsymbol{\theta}_0 \triangleq [J_{11}^0, J_{22}^0, J_{33}^0, 0, 0, 0]^{\mathrm{T}}$, $\boldsymbol{\theta}_\Delta \triangleq [\Delta_{11}, \Delta_{22}, \Delta_{33}, \Delta_{23}, \Delta_{13}, \Delta_{12}]^{\mathrm{T}}$, then equation (30) turns to

$$J\dot{\boldsymbol{s}}_2 = Y(\boldsymbol{\theta}_0 + \boldsymbol{\theta}_\Delta) + J\boldsymbol{n}_2 + \boldsymbol{\tau} + \boldsymbol{d}_\tau \tag{31}$$

where $Y = L(S(\boldsymbol{\omega}_e)(\boldsymbol{\omega}-\boldsymbol{\omega}_e)) - S(\boldsymbol{\omega})L(\boldsymbol{\omega}) - L(\Lambda_2 G(\boldsymbol{\sigma}_e)\boldsymbol{\omega}_e)$.

Denote unknown constant $\rho_J = \|J\|\|J_t^{-1}\|\|J_t\|$, estimation errors $\tilde{\boldsymbol{\theta}}_\Delta = \hat{\boldsymbol{\theta}}_\Delta - \boldsymbol{\theta}_\Delta$, $\tilde{\rho}_J = \hat{\rho}_J - \rho_J$, $\tilde{\rho}_\tau = \hat{\rho}_\tau - \rho_\tau$ and define

$$V_2 = \frac{1}{2}\boldsymbol{s}_2^{\mathrm{T}}J\boldsymbol{s}_2 + \frac{1}{2\gamma_4}\tilde{\boldsymbol{\theta}}_\Delta^{\mathrm{T}}\tilde{\boldsymbol{\theta}}_\Delta + \frac{1}{2\gamma_5}\tilde{\rho}_\tau^2 + \frac{1}{2\gamma_6}\tilde{\rho}_J^2 \tag{32}$$

where $\gamma_i > 0 (i = 4,5,6)$, we obtain

$$\begin{aligned} \dot{V}_2 =& \boldsymbol{s}_2^{\mathrm{T}}J\dot{\boldsymbol{s}}_2 + \frac{1}{\gamma_4}\tilde{\boldsymbol{\theta}}_\Delta^{\mathrm{T}}\dot{\hat{\boldsymbol{\theta}}}_\Delta + \frac{1}{\gamma_5}\tilde{\rho}_\tau\dot{\hat{\rho}}_\tau + \frac{1}{\gamma_6}\tilde{\rho}_J\dot{\hat{\rho}}_J \\ =& \boldsymbol{s}_2^{\mathrm{T}}[Y(\boldsymbol{\theta}_0 + \boldsymbol{\theta}_\Delta) + J\boldsymbol{n}_2 + \boldsymbol{\tau} + \boldsymbol{d}_\tau] \\ &+ \frac{1}{\gamma_4}\tilde{\boldsymbol{\theta}}_\Delta^{\mathrm{T}}\dot{\hat{\boldsymbol{\theta}}}_\Delta + \frac{1}{\gamma_5}\tilde{\rho}_\tau\dot{\hat{\rho}}_\tau + \frac{1}{\gamma_6}\tilde{\rho}_J\dot{\hat{\rho}}_J \end{aligned} \tag{33}$$

Design the relative attitude control input

$$\begin{aligned} \boldsymbol{\tau} =& -K_2\boldsymbol{s}_2 - Y(\boldsymbol{\theta}_0 + \hat{\boldsymbol{\theta}}_\Delta) - \hat{\rho}_\tau\mathrm{sgn}(\boldsymbol{s}_2) \\ &- \hat{\rho}_J\|\boldsymbol{\omega}-\boldsymbol{\omega}_e\|^2\mathrm{sgn}(\boldsymbol{s}_2) \end{aligned} \tag{34}$$

where feedback gain matrix $K_2 = K_2^{\mathrm{T}} > 0$. Substituting (34) into (33) yields

$$\begin{aligned} \dot{V}_2 =& -\boldsymbol{s}_2^{\mathrm{T}}K_2\boldsymbol{s}_2 + \boldsymbol{s}_2^{\mathrm{T}}J\boldsymbol{n}_2 + \boldsymbol{s}_2^{\mathrm{T}}\boldsymbol{d}_\tau - \boldsymbol{s}_2^{\mathrm{T}}Y\tilde{\boldsymbol{\theta}}_\Delta \\ &- \boldsymbol{s}_2^{\mathrm{T}}\hat{\rho}_\tau\mathrm{sgn}(\boldsymbol{s}_2) - \boldsymbol{s}_2^{\mathrm{T}}\hat{\rho}_J\|\boldsymbol{\omega}-\boldsymbol{\omega}_e\|^2\mathrm{sgn}(\boldsymbol{s}_2) \\ &+ \frac{1}{\gamma_4}\tilde{\boldsymbol{\theta}}_\Delta^{\mathrm{T}}\dot{\hat{\boldsymbol{\theta}}}_\Delta + \frac{1}{\gamma_5}\tilde{\rho}_\tau\dot{\hat{\rho}}_\tau + \frac{1}{\gamma_6}\tilde{\rho}_J\dot{\hat{\rho}}_J \end{aligned} \tag{35}$$

Design parameters adaptive update laws as

$$\begin{cases} \dot{\hat{\boldsymbol{\theta}}}_\Delta = \gamma_4 Y^{\mathrm{T}}\boldsymbol{s}_2 \\ \dot{\hat{\rho}}_\tau = \gamma_5\|\boldsymbol{s}_2\|_1 \\ \dot{\hat{\rho}}_J = \gamma_6\|\boldsymbol{\omega}-\boldsymbol{\omega}_e\|^2\|\boldsymbol{s}_2\|_1 \end{cases} \tag{36}$$

then substituting (36) into (35) and considering $\|S(\boldsymbol{a})\| = \|\boldsymbol{a}\|$, $\|R\| = \|R^{\mathrm{T}}\| = 1$, $\|\boldsymbol{s}_2\| \le \|\boldsymbol{s}_2\|_1$ yield

$$\begin{aligned} \dot{V}_2 \le& -\boldsymbol{s}_2^{\mathrm{T}}K_2\boldsymbol{s}_2 + \rho_J\|\boldsymbol{s}_2\|\|R\|\|R^{\mathrm{T}}\|^2\|\boldsymbol{\omega}-\boldsymbol{\omega}_e\|^2 \\ &+ \rho_\tau\|\boldsymbol{s}_2\| - \boldsymbol{s}_2^{\mathrm{T}}Y\tilde{\boldsymbol{\theta}}_\Delta - \hat{\rho}_\tau\|\boldsymbol{s}_2\|_1 - \hat{\rho}_J\|\boldsymbol{s}_2\|_1\|\boldsymbol{\omega}-\boldsymbol{\omega}_e\|^2 \\ &+ \tilde{\boldsymbol{\theta}}_\Delta^{\mathrm{T}}Y^{\mathrm{T}}\boldsymbol{s}_2 + \tilde{\rho}_\tau\|\boldsymbol{s}_2\|_1 + \tilde{\rho}_J\|\boldsymbol{s}_2\|_1\|\boldsymbol{\omega}-\boldsymbol{\omega}_e\|^2 \\ \le& -\boldsymbol{s}_2^{\mathrm{T}}K_2\boldsymbol{s}_2 + \rho_J\|\boldsymbol{\omega}-\boldsymbol{\omega}_e\|^2\|\boldsymbol{s}_2\|_1 + \rho_\tau\|\boldsymbol{s}_2\|_1 \\ &- \hat{\rho}_\tau\|\boldsymbol{s}_2\|_1 - \hat{\rho}_J\|\boldsymbol{\omega}-\boldsymbol{\omega}_e\|^2\|\boldsymbol{s}_2\|_1 \\ &+ \tilde{\rho}_\tau\|\boldsymbol{s}_2\|_1 + \tilde{\rho}_J\|\boldsymbol{\omega}-\boldsymbol{\omega}_e\|^2\|\boldsymbol{s}_2\|_1 \\ =& -\boldsymbol{s}_2^{\mathrm{T}}K_2\boldsymbol{s}_2 \le 0 \end{aligned}$$

and the closed-loop attitude dynamics becomes

$$\begin{aligned} J\dot{\boldsymbol{s}}_2 =& -K_2\boldsymbol{s}_2 - Y\tilde{\boldsymbol{\theta}}_\Delta + J\boldsymbol{n}_2 + \boldsymbol{d}_\tau - \hat{\rho}_\tau\mathrm{sgn}(\boldsymbol{s}_2) \\ &- \hat{\rho}_J\|\boldsymbol{\omega}-\boldsymbol{\omega}_e\|^2\mathrm{sgn}(\boldsymbol{s}_2) \end{aligned} \tag{37}$$

4. STABILITY ANALYSIS

Although above nonlinear robust adaptive controllers are separately designed based on the relative translational and rotational models, stability of the relative motion closed-loop systems under the proposed controllers should be studied uniformly due to the couplings between the translational and rotational motions. The result is described in following theorem.

Theorem 1. Consider the spacecraft proximity operations models (13), (14), (19) and (20), if the relative position and attitude controllers are designed by (25) and (34), corresponding parameter adaptive updating laws are assigned as (27) and (36), respectively; then tracking errors of the closed-loop system asymptotically converge to zero and parameter estimation errors are uniformly bounded.

Proof. Taking $V = V_1 + V_2 \ge 0$ as the Lyapunov function for the closed-loop systems (28) and (37), we know

$$\begin{aligned} \dot{V} &\le -\lambda_{k1}\|\boldsymbol{s}_1\|^2 - \lambda_{k2}\|\boldsymbol{s}_2\|^2 \\ &\le -\mu\|\boldsymbol{s}\|^2 \le 0 \end{aligned} \tag{38}$$

where λ_{k1} and λ_{k2} are the minimum eigenvalues of K_1 and K_2, respectively; $\boldsymbol{s} \triangleq [\boldsymbol{s}_1^{\mathrm{T}}, \boldsymbol{s}_2^{\mathrm{T}}]^{\mathrm{T}}$ and $\mu \triangleq \min\{\lambda_{k1}, \lambda_{k2}\}$.

Since $V(t) \ge 0$ and $\dot{V}(t) \le 0$, $V(t)$ is monotonically decreasing along the closed-loop system trajectory and is bounded by zero. Hence $V(t)$ has a finite limit $V(\infty)$ as $t \to \infty$ and

$$0 \le V(\infty) \le V(t) \le V(0) < \infty, \forall t \ge 0$$

From (38), we know

$$\int_0^\infty \|\boldsymbol{s}\|^2\mathrm{d}t \le -\frac{1}{\mu}\int_0^\infty \dot{V}(t)\mathrm{d}t \le \frac{V(0)-V(\infty)}{\mu} \le \frac{V(0)}{\mu} < \infty$$

This means that $\|\boldsymbol{s}\|$ is square integrable.

Considering the definition of $V(t)$, we have

$$0 \le \frac{1}{2}k_0\|\boldsymbol{r}_e\|^2 + \frac{1}{2}m\|\boldsymbol{s}_1\|^2 + \frac{1}{2}\lambda_J\|\boldsymbol{s}_2\|^2 + \frac{1}{2\gamma}\|\boldsymbol{\zeta}\|^2 \le V(t) < \infty$$

where λ_J is minimum eigenvalue of J, $\boldsymbol{\zeta} \triangleq [\tilde{m}_\Delta, \tilde{\boldsymbol{\theta}}_\Delta^{\mathrm{T}}, \tilde{\rho}_f, \tilde{\rho}_\tau, \tilde{\rho}_m, \tilde{\rho}_J]^{\mathrm{T}}$, and $\gamma \triangleq \max\{\gamma_1, \gamma_2, \gamma_3, \gamma_4, \gamma_5, \gamma_6\}$. It follows that $\|\boldsymbol{r}_e\| < \infty$, $\|\boldsymbol{s}\| < \infty$ and $\|\boldsymbol{\zeta}\| < \infty$. Since $\|R\| = 1$, $\|\boldsymbol{\sigma}_e\| \le 1$, from (21) and (29), we know that $\|\boldsymbol{v}_e\| = \|\boldsymbol{s}_1 - \Lambda_1\boldsymbol{r}_e\| < \infty$, $\|\boldsymbol{\omega}_e\| = \|\boldsymbol{s}_2 - \Lambda_2\boldsymbol{\sigma}_e\| < \infty$; and considering (11), (12), Claim 1, we can obtain $\|\boldsymbol{v}\| = \|\boldsymbol{v}_e + R[\boldsymbol{v}_t + S(\boldsymbol{\omega}_t)\boldsymbol{p}_t]\| < \infty$, $\|\boldsymbol{\omega}\| = \|\boldsymbol{\omega}_e + R\boldsymbol{\omega}_t\| < \infty$. Furthermore, from (19), (20), (25) and (34), we know $\|\boldsymbol{f}\| < \infty$ and $\|\boldsymbol{\tau}\| < \infty$; from (28) and (37), we have $\|\dot{\boldsymbol{s}}\| < \infty$, which implies that $\|\boldsymbol{s}\|$ is uniformly continuous. Then, based on the Barbalat Lemma (Krstic et al. (1995)), we conclude $\lim_{t\to\infty}\boldsymbol{s}_1 = \lim_{t\to\infty}\boldsymbol{s}_2 = \boldsymbol{0}$.

On the manifolds $\boldsymbol{s}_1 = \boldsymbol{v}_e + \Lambda_1\boldsymbol{r}_e = \boldsymbol{0}$ and $\boldsymbol{s}_2 = \boldsymbol{\omega}_e + \Lambda_2\boldsymbol{\sigma}_e = \boldsymbol{0}$, we have $\dot{\boldsymbol{r}}_e + [\Lambda_1 + S(\boldsymbol{\omega})]\boldsymbol{r}_e = \boldsymbol{0}$ and $\dot{\boldsymbol{\sigma}}_e + G(\boldsymbol{\sigma}_e)\Lambda_2\boldsymbol{\sigma}_e = \boldsymbol{0}$ from (13) and (14), then we chose a Lyapunov function

$$V_s = \frac{1}{2}\boldsymbol{r}_e^{\mathrm{T}}\boldsymbol{r}_e + \frac{1}{2}\boldsymbol{\sigma}_e^{\mathrm{T}}\boldsymbol{\sigma}_e \ge 0$$

Taking time derivative along the manifolds with $\boldsymbol{r}_e^{\mathrm{T}}S(\boldsymbol{\omega})\boldsymbol{r}_e = 0$ and considering $\boldsymbol{\sigma}_e^{\mathrm{T}}G(\boldsymbol{\sigma}_e) = \dfrac{1+\boldsymbol{\sigma}_e^{\mathrm{T}}\boldsymbol{\sigma}_e}{4}\boldsymbol{\sigma}_e^{\mathrm{T}}$(Shuster (1993)) yield

$$\begin{aligned}\dot{V}_s =& \boldsymbol{r}_e^{\mathrm{T}}\dot{\boldsymbol{r}}_e + \boldsymbol{\sigma}_e^{\mathrm{T}}\dot{\boldsymbol{\sigma}}_e \\ =& -\boldsymbol{r}_e^{\mathrm{T}}[\Lambda_1 + S(\boldsymbol{\omega})]\boldsymbol{r}_e - \boldsymbol{\sigma}_e^{\mathrm{T}}G(\boldsymbol{\sigma}_e)\Lambda_2\boldsymbol{\sigma}_e \\ =& -\boldsymbol{r}_e^{\mathrm{T}}\Lambda_1\boldsymbol{r}_e - \frac{1+\boldsymbol{\sigma}_e^{\mathrm{T}}\boldsymbol{\sigma}_e}{4}\boldsymbol{\sigma}_e^{\mathrm{T}}\Lambda_2\boldsymbol{\sigma}_e \\ \leq& -\lambda_{m1}\|\boldsymbol{r}_e\|^2 - \frac{\lambda_{m2}}{4}\|\boldsymbol{\sigma}_e\|^2 \leq 0\end{aligned} \tag{39}$$

where λ_{m1} and λ_{m2} are minimum eigenvalues of Λ_1 and Λ_2, respectively. So $V_s(t)$ is monotonically decreasing and bounded on the manifolds, it follows that it has a finite limit $V_s(\infty)$ as $t \to \infty$ such that $0 \leq V_s(\infty) \leq V_s(t) \leq V_s(0) < \infty$ for all $t \geq 0$. This means that $\|\boldsymbol{r}_e\|$ and $\|\boldsymbol{\sigma}_e\|$ are bounded, and from (39) we can prove $\int_0^\infty \|\boldsymbol{r}_e\|^2 \mathrm{d}t < \infty$ and $\int_0^\infty \|\boldsymbol{\sigma}_e\|^2 \mathrm{d}t < \infty$. From $\|\boldsymbol{r}_e\| < \infty$, $\|\boldsymbol{\sigma}_e\| \leq 1$, $\|\boldsymbol{s}\| < \infty$, (21), (29), we get $\|\boldsymbol{v}_e\| < \infty$, $\|\boldsymbol{\omega}_e\| < \infty$; from (12) and Claim 1 we know $\|\boldsymbol{\omega}\| < \infty$. Then from (13) and (14), we have $\|\dot{\boldsymbol{r}}_e\| < \infty$ and $\|\dot{\boldsymbol{\sigma}}_e\| < \infty$. It implies that $\boldsymbol{r}_e$ and $\boldsymbol{\sigma}_e$ are uniformly continuous. Based on the Barbalat Lemma, we know $\lim_{t\to\infty}\boldsymbol{r}_e = \lim_{t\to\infty}\boldsymbol{\sigma}_e = \boldsymbol{0}$.

Furthermore, from (21), (29) and $\lim_{t\to\infty}\boldsymbol{s}_1 = \lim_{t\to\infty}\boldsymbol{s}_2 = \boldsymbol{0}$, we know $\lim_{t\to\infty}\dot{\boldsymbol{r}}_e = \lim_{t\to\infty}\dot{\boldsymbol{\sigma}}_e = \boldsymbol{0}$. Thus, according to (13), (14) and considering $G(\boldsymbol{\sigma}_e)$ is invertible, we conclude $\lim_{t\to\infty}\boldsymbol{v}_e = \lim_{t\to\infty}\boldsymbol{\omega}_e = \boldsymbol{0}$.

Claim 3. It should be noted that the gain matrices $\{K_1, \Lambda_1\}$ in the relative position controller and $\{K_2, \Lambda_2\}$ in the relative attitude controller can be designed independently to satisfy their own bandwidths, respectively.

5. SIMULATION AND DISCUSSION

In this section, an autonomous proximity mission in orbit for rendezvous and docking is simulated. The tumbling target spacecraft has a smaller initial dynamic condition of position and attitude so that the successive docking operations can be effectively carried out and achieved. After the relative position and relative attitude between two spacecrafts are precisely controlled, subsequent docking operations can be safely realized. Simulation results are presented to demonstrate the performance of the developed controllers.

Initial values in the simulation are shown in Table 1. The desired position for chaser in frame $\mathscr{F}_t$ is $\boldsymbol{p}_t = [0,5,0]^{\mathrm{T}}(\mathrm{m})$. The nominal values of the chaser mass and inertial parameters are $m_0 = 50(\mathrm{kg})$ and $\boldsymbol{\theta}_0 = [580,400,300,0,0,0]^{\mathrm{T}}(\mathrm{kgm}^2)$, respectively. We use the proposed controllers to achieve the spacecraft proximity operations. The controller parameters are chosen as $k_0 = 0.1$, $K_1 = 20I_3$, $K_2 = 100I_3$, $\Lambda_1 = 0.05I_3$, $\Lambda_2 = 0.2I_3$, $\gamma_i = 0.02(i = 1,\cdots,6)$, $\hat{m}_\Delta(0) = \hat{\rho}_f(0) = \hat{\rho}_\tau(0) = \hat{\rho}_m(0) = \hat{\rho}_J(0) = 0$, $\hat{\boldsymbol{\theta}}_\Delta(0) = \boldsymbol{0}$.

In the simulation, parameters of the chaser, the target and disturbances are listed as follows:

$$m = 58.2(\mathrm{kg}),\ J = \begin{bmatrix} 598.3 & -22.5 & -51.5 \\ -22.5 & 424.4 & -27 \\ -51.5 & -27 & 263.6 \end{bmatrix}(\mathrm{kgm}^2)$$

$$J_t = \begin{bmatrix} 3336.3 & -135.4 & -154.2 \\ -135.4 & 3184.5 & -148.5 \\ -154.2 & -148.5 & 2423.7 \end{bmatrix}(\mathrm{kgm}^2)$$

$$\boldsymbol{d}_\tau = \begin{bmatrix} 1+\sin(\frac{\pi t}{125})+\sin(\frac{\pi t}{200}) \\ 1+\sin(\frac{\pi t}{125})+\sin(\frac{\pi t}{250}) \\ 1+\cos(\frac{\pi t}{125})+\cos(\frac{\pi t}{250}) \end{bmatrix} \times 10^{-2}(\mathrm{Nm})$$

$$\boldsymbol{d}_f = \begin{bmatrix} 1+\sin(\frac{\pi t}{125})+\sin(\frac{\pi t}{200}) \\ 1+\sin(\frac{\pi t}{125})+\sin(\frac{\pi t}{250}) \\ 1+\cos(\frac{\pi t}{125})+\cos(\frac{\pi t}{250}) \end{bmatrix} \times 10^{-2}(\mathrm{N})$$

The simulation results of relative attitude are shown in Figure 2, including the relative attitude, relative angular velocity and control torques represented in frame $\mathscr{F}_c$. These results demonstrate a good attitude tracking performance: the attitude synchronization is achieved in about 80(s) and the relative attitude converges to zero, which indicates that the chaser attitude is synchronized with the target attitude. Figure 3 shows the simulation results of relative position, relative velocity and control forces expressed in frame $\mathscr{F}_c$ for controlling the chaser to a desired position $\boldsymbol{p}_t = [0,5,0]^{\mathrm{T}}(\mathrm{m})$ in frame $\mathscr{F}_t$. As shown in Figure 3, the desired position tracking is accomplished in about 100(s) and the relative position converges to zero. The control forces and the control torques presented in Figure 2 and Figure 3 show that the large control efforts of chaser spacecraft are used initially in order to track the desired proximity position and coincide with the tumbling target attitude quickly. Moreover, after the desired position and attitude are achieved, the control efforts decrease rapidly. Small oscillations of control forces and torques are preserved as shown in Figure 2 and Figure 3, because of the control inputs for tracking the target motions and suppressing the modeling uncertainties. Figure 4 and Figure 5 show that the adaptive estimated values for the unknown parameters are all bounded. The simulation results demonstrate that the proposed control strategy for chaser spacecraft can track the target motions precisely and asymptotic stability of the closed-loop system can be guaranteed.

Table 1. Initial values in simulation

Variable	Value	Unit
$\boldsymbol{r}$	$[1,1,1]^{\mathrm{T}} \times 7.078 \times 10^6$	m
$\boldsymbol{v}$	$[0,0,0]^{\mathrm{T}}$	m/s
$\boldsymbol{\sigma}$	$[0,0,0]^{\mathrm{T}}$	rad
$\boldsymbol{\omega}$	$[0,0,0]^{\mathrm{T}}$	rad/s
$\boldsymbol{r}_e$	$[50/\sqrt{2},0,-50/\sqrt{2}]^{\mathrm{T}}$	m
$\boldsymbol{v}_e$	$[0.5,-0.5,0.5]^{\mathrm{T}}$	m/s
$\boldsymbol{\sigma}_e$	$[0.5,-0.6,0.7]^{\mathrm{T}}$	rad
$\boldsymbol{\omega}_e$	$[0.02,-0.02,0.02]^{\mathrm{T}}$	rad/s

6. CONCLUSIONS

In this paper, the control problem of spacecraft proximity operations is investigated. The couplings of translational and rotational dynamics, uncertain inertial parameters and bounded external disturbances are considered in the six degrees-of-freedom relative motion model. A nonlinear robust adaptive state feedback control approach is developed to design relative position and attitude controllers without using the target inertial parameter information. Based on the six degrees-of-freedom relative motion model it is proved that the chaser can track both the target attitude and desired relative position, and the tracking errors converge to zero.

Future works of this research include: 1) extending the proposed controller to more practical cases, such as finite time docking, control inputs constraints, and measurement noise et al; 2) redesigning the controller for the flexible chaser and target spacecrafts in proximity operations.

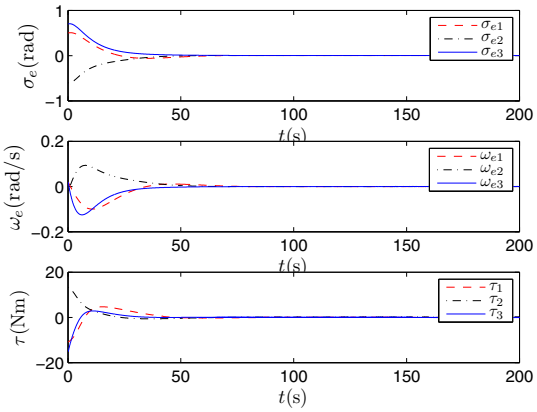

Fig. 2. Time history for relative attitude motion

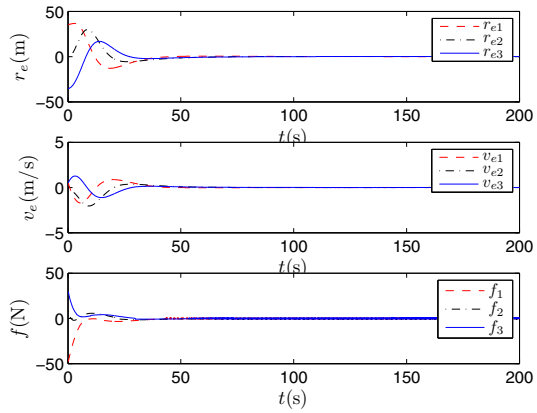

Fig. 3. Time history for relative position motion

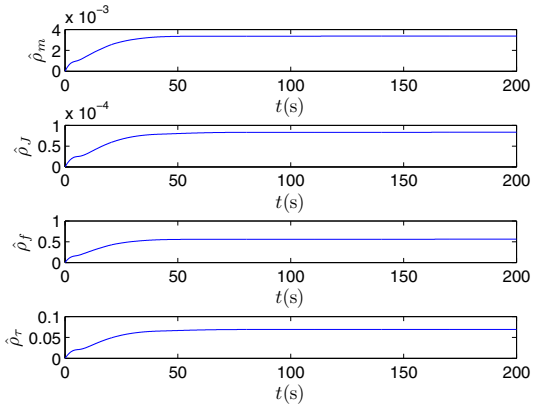

Fig. 4. Time history for estimated parameters

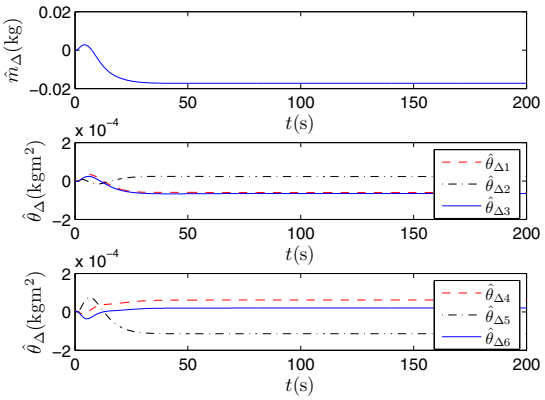

Fig. 5. Time history for estimated parameters

REFERENCES

D. T. Stansbery, J. R. Cloutier. Position and attitude control of a spacecraft using the state dependent riccati equation technique. *Proceedings of the American Control Conference*, pages 1867–1871, 2000.

F. Zhang, G. Duan, M. Hou. Integrated relative position and attitude control of spacecraft in proximity operation missions with control saturation. *International Journal of Innovative Computing, Information and Control*, 8:1–14, 2012.

I. Yuichi, K. Takashi, N. Tomoyuki. Nonlinear tracking control of rigid spacecraft under disturbance using PD and PID type $\mathscr{H}_\infty$ state feedback. *Proceedings of the 50th IEEE Conference on Decision and Control and European Control Conference*, pages 6184–6191, 2011.

J. Liang, O. Ma. Angular velocity tracking for satellite rendezvous and docking. *Acta Astronautica*, 69:1019–1028, 2011.

K. Subbarao, S. Welsh. Nonlinear control of motion synchronization for satellite proximity operations. *Journal of Guidance, Control and Dynamics*, 31:1284–1294, 2008.

M. D. Shuster, A survey of attitude representations. *The Journal of the Astronautical Sciences*, 41:439–517, 1993.

M. Krstic, I. Kanellakopoulos, P. Kokotovic. *Nonlinear and Adaptive Control Design*. NY: John Wiley & Sons, 1995.

M. D. Lither, S. Dubowsky. State, shape and parameter estimation of space objects from range images. *Proceedings of the 2004 IEEE International Conference on Robotics and Automation*, pages 2974–2979, 2004.

M. Xin, H. Pan. Integrated nonlinear optimal control of spacecraft in proximity operations. *International Journal of Control*, 83:347–363, 2010.

M. Xin, H. Pan. Nonlinear optimal control of spacecraft approaching a tumbling target. *Aerospace Science and Technology*, 15: 79–89, 2011.

M. Xin, H. Pan. Indirect robust control of spacecraft via optimal control solution. *IEEE Transactions on Aerospace and Electronic Systems*, 48:1798–1809, 2012.

N. K. Philip, M. R. Ananthasayanam. Relative position and attitude estimation and control schemes for the final phase of an autonomous docking mission of spacecraft. *Acta Astronautica*, 52:511–522, 2003.

P. Singla, K. Subbarao, J. L. Junkins. Output feedback based adaptive control for spacecraft rendezvous and docking under measurement uncertainties. *Journal of Guidance, Control, and Dynamics*, 29:892–902, 2006.

S. Di Cairano, H. Park, I. Kolmanovsky. Model predictive control approach for guidance of spacecraft rendezvous and proximity maneuvering. *International Journal of Robust and Nonlinear Control*, 22:1398–1427, 2010.

Z. Meng, W. Ren, Z. You. Decentralised cooperative attitude tracking using modified Rodriguez parameters based on relative attitude information. *International Journal of Control*, 83:2427–2439, 2010.